ELSEVIER

Biophysical Chemistry 122 (2006) 66–73

Biophysical Chemistry

http://www.elsevier.com/locate/biophyschem

An EPR study of the interfacial properties of phosphatidylcholine vesicles with different lipid chain lengths

Marilene Alves, Miroslav Peric *

Department of Physics and Astronomy and The Center for Supramolecular Studies, California State University at Northridge, Northridge, CA 91330-8268, United States

Received 10 January 2006; received in revised form 9 February 2006; accepted 9 February 2006
Available online 23 February 2006

Abstract

The hydrophobic spin probe 2,2,6,6-tetramethyl-piperidin-1-oxyl-4-yl octadecanoate (TEMPO-stearate) is used to study the interfacial properties of a variety of phosphatidylcholine vesicles. Since the spin probe exhibits a fast motional electron paramagnetic resonance (EPR) spectrum above the phase transition, the EPR spectrum of the spin probe is analyzed by nonlinear least-squares spectral fitting. EPR spectral line fitting provides high precision spectral parameters, which can be used to construct a detailed picture of the dynamics of the probe and its environment. The hyperfine coupling spacing is used to estimate the effective water concentration in the polar shell of vesicles, while the rotational correlation times give the information on the motion of the spin probe. The effective water concentration of the polar shell of dimyristoyl-phosphatidylglycerol (DMPG) vesicles is greater on average by about 4.0 M than the effective water concentration of the polar shell of dimyristoyl-phosphatidylcholine (DMPC) vesicles. The effective water concentration decreases by about 0.5 M for an increase of two carbons in the chain, and increases noticeably with hydrocarbon chain unsaturation, which is in good agreement with literature values. The nitroxide moiety rotates preferentially along the N–O bond, that is, parallel to its hydrocarbon chain.

Keywords: Electron paramagnetic resonance (EPR) spectroscopy; Spin probes; Nonlinear least-squares spectral line fitting; Phosphatidylcholine vesicles; Vesicle surface hydration

1. Introduction

During the last four decades, application of electron paramagnetic resonance (EPR) spectroscopy together with the spin probe (label) method has enormously contributed to our current understanding of biological membranes [1–3]. Since spin probes can be tailored for a particular experiment, a wide variety of spin probes including fatty acid spin probes, phospholipid spin probes and various TEMPO (2,2,6,6-tetramethyl-1-piperidinyloxy) derivatives have been used in membrane studies. The physicochemical properties of the membrane interface play a crucial role in various bio-interfacial phenomena such as immobilization of enzymes in biocatalysis, phagocytosis, membrane fusion, diffusion and transport of biomembranes [4,5]. Due to the position of the nitroxide spin probe TEMPO at the end of a long hydrocarbon chain, Scheme 1, the long chain TEMPO derivatives are extremely well suited to study the interface properties of membranes [6–10], as well as other self-assembled aggregates such as micelles [11]. The hydrophobicity of the hydrocarbon chain ensures that NO· resides in the hydration layer of the aggregate.

In recent years, nonlinear least-squares spectral fitting of the fast motion EPR spectrum of spin labels in solution has become an important data analysis method in EPR spectroscopy [12–15]. Although EPR line positions and line widths can be measured directly from the EPR spectrum using conventional methods, EPR spectral line fitting offers one a series of benefits: (1) increased accuracy and precision in the determination of EPR line parameters; (2) an increased signal-to-noise ratio; (3) extraction of the homogeneous Lorentzian linewidth from an inhomogeneously broadened EPR line; and (4) access to EPR parameters otherwise not readily available. Item (1) enables one at least one order of magnitude increase in precision in the

* Corresponding author. Tel.: +1 818 677 2944; fax: +1 818 677 3234.
E-mail address: miroslav.peric@csun.edu (M. Peric).

0301-4622/$ - see front matter © 2006 Elsevier B.V. All rights reserved.
doi:10.1016/j.bpc.2006.02.003

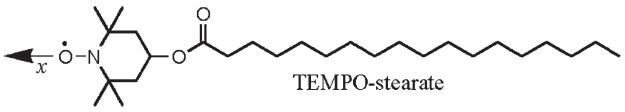

Scheme 1. Schematic representation of TEMPO-stearate probe.

measurements of both EPR line positions and linewidths. By using the observed linewidth measured directly from the EPR spectrum instead of the Lorentzian linewidth, item (3), the errors in the determination of correlation times may be up to 30% [16]. Due to these obvious benefits [17] fast motion EPR spectral fitting, in combination with hydrophobic EPR spin probes, has been successfully applied to study the physicochemical properties of the micelle interface [18–20]. In the case of membranes and vesicles, most hydrophobic spin probes usually exhibit restricted motion giving rise to a slow motion EPR spectrum which can still be fitted using computer simulation techniques developed by Freed [21,22]. Unfortunately, these computer simulations require a large number of adjustable parameters which introduce ambiguities and reduce precision. Thus, EPR spectral fitting in model membranes has so far been done only by utilizing small spin probes having fast motion EPR spectra [23,24]. Unlike most hydrophobic spin probes, long chain TEMPO derivatives undergo fast rotational motion above the lipid phase transition, because NO· resides in the hydration layer of the membrane which is more fluid than the hydrocarbon bilayer region. Consequently, long chain TEMPO derivatives are good candidates for studying the hydration properties of the membrane interface above the phase transition using fast motion EPR spectral fitting.

This work has two objectives: (1) to demonstrate that spectral fitting may be successfully applied to the EPR spectrum of the spin probe 2,2,6,6-tetramethyl-piperidin-1-oxyl-4-yl octadecanoate (TEMPO-stearate) in phospholipid vesicles above the phase transition, yielding EPR parameters of high precision that can be used to construct a detailed picture of the spin probe motion and its environment, and (2) to apply the fitting method to study the effect of acyl chain length on the physicochemical properties of the hydration layer of phosphatidylcholine vesicles.

2. Materials and methods

2.1. Materials

The phospholipids DMPC (1,2-dimyristoyl-sn-glycero-3-phosphocholine), DPPC (1,2-dipalmitoyl-sn-glycero-3-phosphocholine), DSPC (1,2-distearoyl-sn-glycero-3-phosphocholine) and DOPC (1,2-dioleoyl-sn-glycero-3-phosphocholine) were purchased from Avanti Polar Lipids (Birmingham, AL, USA) and used as received. The spin label 2,2,6,6-tetramethyl-piperidin-1-oxyl-4-yl octadecanoate (TEMPO-stearate) was obtained from Molecular Probes, Inc. (Eugene, OR).

The buffer used was 20 mM Hepes buffer (4-(2-hydroxyethil)-1-piperizineethanesulfonic acid) adjusted to pH 7.4 with NaOH (sodium hydroxide from Sigma). PTFE tubing was a gift from Fluortek (Easton, PA, USA).

2.2. Lipid dispersion preparation

The appropriate amount of TEMPO-stearate chloroform solution was added to phospholipid powder to produce a molar ratio [lipid]/[spin probe] of 400. The completely clear solution was dried under a stream of N_2. Thereafter, the dried films were kept under reduced pressure overnight to guarantee complete absence of chloroform. The phospholipid films were hydrated by the addition of Hepes aqueous solution until a 100 mM concentration of lipid was achieved. After 20 min of vortexing, opaque suspensions were obtained. The suspensions were finally transferred into PTFE (PolyTetraFluoroEthylene) capillary tubes, whose ends were folded and tightened with parafilm (American National Can, Greenwich, CT).

2.3. EPR spectroscopy

EPR experiments were performed with a Bruker ESP 300 E spectrometer equipped with a Bruker variable temperature unit (Model B-VT-2000). The PTFE tube with the fresh vesicle suspension was inserted in a standard 4 mm diameter EPR quartz (Wilmad Glass Co Cat No. 412) with a hole in the bottom to allow nitrogen equilibration of the sample [25]. This arrangement deoxygenates the sample reducing the broadening of the EPR lines caused by molecular oxygen. The thermocouple tip was placed in just outside of the sensitive region of the cavity. The sample temperature was measured with an Omega temperature indicator (model DP41-TC-S2), and it was stable within ±0.2 °C. Samples were equilibrated for at least 5 min at each temperature and measurements were performed starting from temperatures around the phase transition, except for DOPC because its phase transition temperature is around −19.5 °C. In order to avoid any problems due to sample aging, dispersion was freshly prepared and measured on the same day.

Five first harmonic EPR spectra were obtained for each temperature using a sweep time of 84 s; microwave power, 5 mW; time constant, 20.5 ms; sweep width, 50.2 G; modulation amplitude, 1 G. Since the EPR lines are inhomogeneously broadened due to unresolved hyperfine interaction, the EPR spectra were then analyzed by the computer program Lowfit which performs nonlinear least-squares fitting of the experimental EPR spectrum using a model of a Lorentzian–Gaussian sum function, exploiting the fact that such a sum is an excellent approximation of the Voigt shape [12,16]. This analysis separates the Lorentzian and Gaussian contributions to the observed spin probe lines, so that the Lorentzian linewidth can be used in the calculation of the rotational correlation times as described previously in Ref. [16]. The latest version of Lowfit has a fitting option which incorporates the dispersion EPR line shape in the fitting function, so it can easily detect any spin exchange in the EPR spectrum [14,26].

Information on molecular motions of a spin probe may be obtained from the line shape analysis of the spin probe's EPR spectrum. In fast motion regime, the peak-to-peak Lorentzian linewidth of an individual hyperfine component is:

$$\Delta H_{pp}^{L}(m) = A + Bm + Cm^2, \quad (1)$$

where m is the z component of the nitrogen nuclear spin. The parameters A, B, and C depend on the magnitude and rate of modulation of the magnetic anisotropies by the molecular rotational motion. Term A contributes equally to all three lines, and includes contributions other than motional [27]. Experimentally, A is the peak-to-peak Lorentzian linewidth of the central line, $\Delta H^{L}_{pp}(0)$, and terms B and C are given by:

$$B = \frac{1}{2}\Delta H^{L}_{pp}(0)\left\{\frac{\Delta H^{L}_{pp}(+1)}{\Delta H^{L}_{pp}(0)} - \frac{\Delta H^{L}_{pp}(-1)}{\Delta H^{L}_{pp}(0)}\right\} \quad (2a)$$

$$C = \frac{1}{2}\Delta H^{L}_{pp}(0)\left\{\frac{\Delta H^{L}_{pp}(+1)}{\Delta H^{L}_{pp}(0)} + \frac{\Delta H^{L}_{pp}(-1)}{\Delta H^{L}_{pp}(0)} - 2\right\} \quad (2b)$$

where $\Delta H^{L}_{pp}(+1)$ and $\Delta H^{L}_{pp}(-1)$ are the peak-to-peak Lorentzian linewidths of the low- and high-field lines.

For anisotropic Brownian rotational motion which is axially symmetric about one of the spin probe's axes, one needs two independent rotational correlation times. One of the rotational correlation times $\tau_{||}$ characterizes the rotation of the spin probe about the molecular symmetry axis, while the second rotational correlation time $\tau_{\perp}$ characterizes the rotation perpendicular to it. The preferred axis of rotation of the probe can be determined by its shape. In the case of TEMPO-stearate, Scheme 1, we expect the probe to rotate about an axis parallel to the hydrocarbon chain, or in terms of the nitroxide principal axis about its x axis, which is along the direction of the N–O bond in its all trans conformation.

For anisotropic rotation which is axially symmetric about the nitroxide x axis, the correlation times can be calculated from the following equations [28]:

$$\tau_{20} = \frac{1.11 \times 10^{-7}}{H(\Delta A)} \frac{5(\delta A)B - 8(\delta g)HC}{(\Delta g)(\delta A) - (\delta g)(\Delta A)} \quad (3)$$

$$\tau_{22} = \frac{3.69 \times 10^{-8}}{H(\delta A)} \frac{8(\Delta g)HC - 5(\Delta A)B}{(\Delta g)(\delta A) - (\delta g)(\Delta A)} \quad (4)$$

where H is the magnetic field, and the hyperfine anisotropies ΔA and δA are given by:

$$\Delta A = A_{xx} - \frac{1}{2}(A_{yy} + A_{zz}) \quad (5)$$

$$\delta A = \frac{1}{2}(A_{yy} - A_{zz}) \quad (6)$$

and similar equations for Δg and δg. All the above quantities are measured in gauss. To the best of our knowledge, there are no measurements of the principal components of g and hyperfine tensors for TEMPO-stearate, so we use the principal components of g and hyperfine tensor values of 4-hydroxi-2,2,6,6-tetramethyl-piperidine (TEMPO) in single crystal [29]. We expect that the principal values of the two spin probes are not much different, since the electron charge density of the nitroxide should not be affected by the hydrocarbon chain. The principal components of g tensor values are $g_{xx}=2.0099$, $g_{yy}=2.0061$ and $g_{zz}=2.0024$, while the principal components of hyperfine values are $A_{xx}=5.3$ G, $A_{yy}=7$ G and $A_{zz}=35$ G. Using these values and assuming the magnetic field to be 3300 G, we get

$$\tau_{20} = -2.969\ B - 2.09\ C\ \text{(ns)} \quad (7)$$

$$\tau_{22} = 1.241\ B + 2.38\ C\ \text{(ns)} \quad (8)$$

The rotational correlation times $\tau_{||}$ and $\tau_{\perp}$ are then given by [28]:

$$\tau_{\perp} = \tau_{20} \quad (9)$$

$$\tau_{||} = \frac{2\tau_{20}\tau_{22}}{3\tau_{20} - \tau_{22}}. \quad (10)$$

3. Results and discussion

Representative EPR spectra of TEMPO-stearate in vesicle dispersions of DMPC at 22, 30 and 50 °C are shown in Fig. 1. Fits of EPR spectra in phosphatidylcholine vesicles above the gel–liquid crystal phase transition are excellent, as can be seen in Fig. 2, which shows both the fit and experimental EPR spectrum of TEMPO-stearate in 100 mM DMPC vesicles at 25 °C, which is only one degree above the phase transition for DMPC vesicle, 24 °C [30]. The fit and experimental spectra are indistinguishable. The excellence of the fit is further supported by the lack of significant residuals, Fig. 2b. This also indicates that the EPR lines are symmetrical with respect to the baseline, meaning that there is no probe ordering in the vesicle [27]. As expected, below the phase transition the motion of the spin probe starts becoming moderately restricted. The EPR spectra can still be fitted with the Lowfit program but their fits, although acceptable, are not as good as the fits of EPR spectra taken above the phase transition. For that reason we analyzed only EPR spectra within 3 °C below the phase transition. Also, the shape of the EPR spectrum with the low-field line taller than the center-field line clearly indicates that the preferred axis of rotation is the molecular x axis, in other words, the TEMPO-stearate molecule undergoes anisotropic rotation which is axially symmetric about the N–O bond, that is, the hydrocarbon chain.

The fact that the TEMPO-stearate gives rise to a fast motion EPR spectrum as shown in Figs. 1 and 2 clearly indicates that

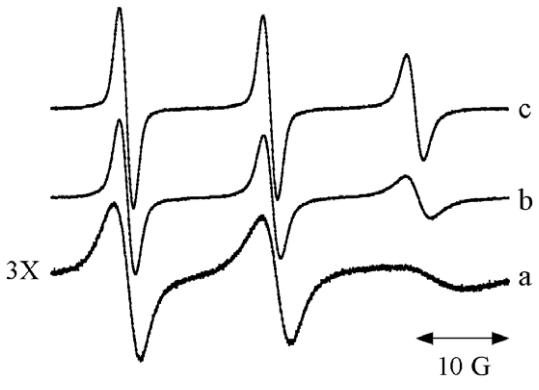

Fig. 1. EPR spectra of 0.2 mM TEMPO-stearate in 100 mM DMPC vesicles in Hepes buffer equilibrated with nitrogen at: a) 22 °C, b) 30 °C and c) 55 °C.

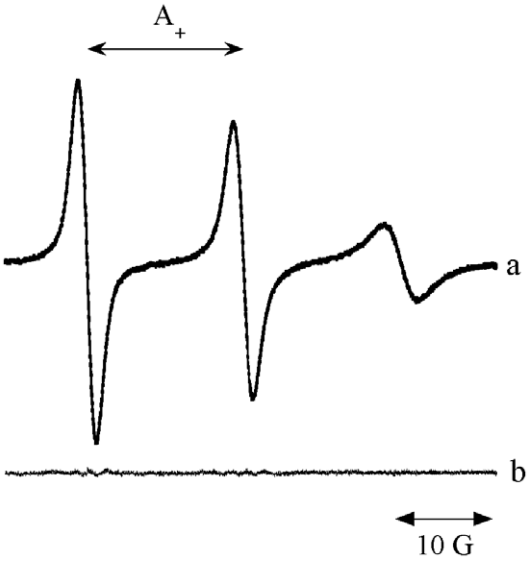

Fig. 2. (a) Experimental EPR spectrum of 0.2 mM TEMPO-stearate in 100 mM DMPC vesicles in Hepes buffer equilibrated with nitrogen at 25 °C. The definition of the nitrogen hyperfine spacing A_+ is also shown. (b) Difference in the best fit and the experimental spectrum.

TEMPO rotation does not reflect the motion of the whole TEMPO-stearate molecule. There is no doubt that the nitroxide which is attached to the hydrocarbon chain by the C–O bond, Scheme 1, can rotate quite freely in all directions, even about the perpendicular axis, so Eq. (9) can be applied [31]. On the other side, sterol analogue spin probes such as cholestane spin-label (CSL) and androstane spin-label (ASL), whose motion in the membrane can be treated as Brownian rotational diffusion of a rigid rod within the confines of a cone, give rise to a rigid limit spectrum [32,33].

It is well established that hyperfine coupling spacing A_+ of a nitroxide, Fig. 2a, is sensitive to the amount of water in the surroundings of the nitroxide [18,24,34]. Solutions of TEMPO-stearate were prepared in a series of mixtures of ethanol–water and ethanol–1,4-dioxane. The hydration index H of each solution mixture [35] defined as the ratio of the molar concentration of OH dipoles in the solution mixture to that of pure water is calculated according to Eq. (5) from Ref. [24]. In the ethanol–water mixture series, the lowest H is that of pure ethanol which is 0.308, thus to cover the hydration index values from zero to 0.308 we chose the mixtures of 1,4-dioxane and ethanol. The mean values of five EPR measurements of A_+ in each mixture are shown in Fig. 3 as a function of H (25 °C). Fitting the data to a line gives $A_+ = 15.542 + 1.297\ H$ with a coefficient of correlation $r = 0.994$ over the range H (25 °C) = 0–0.8. Measurements were also made in the solvent mixtures at 35, 45 and 55 °C, and it was found that the variation in A_+ is negligible. Assuming that at 25 °C the concentration of pure water is 55.345 M, the measured hyperfine coupling spacing A_+ can be then converted into the effective water concentration $[H_2O]$ using the equation:

$$[H_2O] = \frac{A_+ - 15.542}{1.297} 55.345\ (\mathrm{M}) \qquad (11)$$

The hyperfine coupling spacing A_+ in the polar shell of the vesicle and corresponding effective water concentration $[H_2O]$ sensed by TEMPO in a series of phosphatidylcholine vesicles with phospholipids of different acyl chain lengths from 14 to 18 carbons and the lipid DOPC having unsaturated 18 carbon acyl chains as a function of temperature are shown in Fig. 4a. The phase transition for each phospholipid except DOPC can be clearly observed: and their values are within 1 °C of the values reported in the literature [30]. The phase transition of DOPC, −19.5 °C, is well below the temperature range, 0 to 70 °C, in which the EPR spectra of DOPC were taken. Fig. 4b, which is an expanded representation at higher temperatures, clearly shows that the nitrogen hyperfine spacing decreases with chain length and increases with chain unsaturation. Fig. 4b illustrates the benefits of EPR spectral fitting quite well. With the precision of 0.1 G which is usually achieved by conventional methods, see Fig. 5a in Ref. [36], we would not be able to separate the hyperfine spacings of TEMPO-stearate in DMPC, DPPC and DSPC vesicles at all. As can be seen from Fig. 4b, the data points representing the values of hyperfine spacings in phospholipid vesicles, as well as the lines drawn through them, are clearly separated.

Also, for each phospholipid, the value of A_+ below the phase transition increases sharply, clearly indicating the phospholipid phase transition, Fig. 4a. Above the phase transition, as the temperature increases the hyperfine coupling spacing decreases, in other words the effective water concentration decreases. This behavior can be easily explained with the position of the nitroxide in the polar shell of the vesicle. In the gel phase the phospholipid molecules are close to each other, so the molecule of TEMPO-stearate is extended with the N–O moiety very likely located near the surface of the bilayer. In the liquid crystal phase, there is more space between the head groups of phospholipid molecules, so the N–O moiety is pulled deeper into the polar shell. Obviously, the location of TEMPO changes with temperature, indicating that we should be very careful how to interpret the effective water concentration measured by

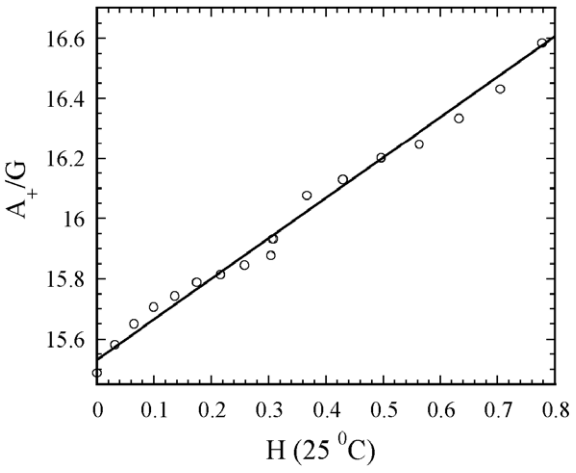

Fig. 3. Nitrogen hyperfine spacing A_+ for TEMPO-stearate as a function of hydrophilicity index H (25 °C) in a series of ethanol–water and ethanol–1,4-dioxane mixtures. The solid line is a linear least-squares fit to the data. $A_+ = 15.542 + 1.297\ H$ (correlation coefficient = 0.9941).

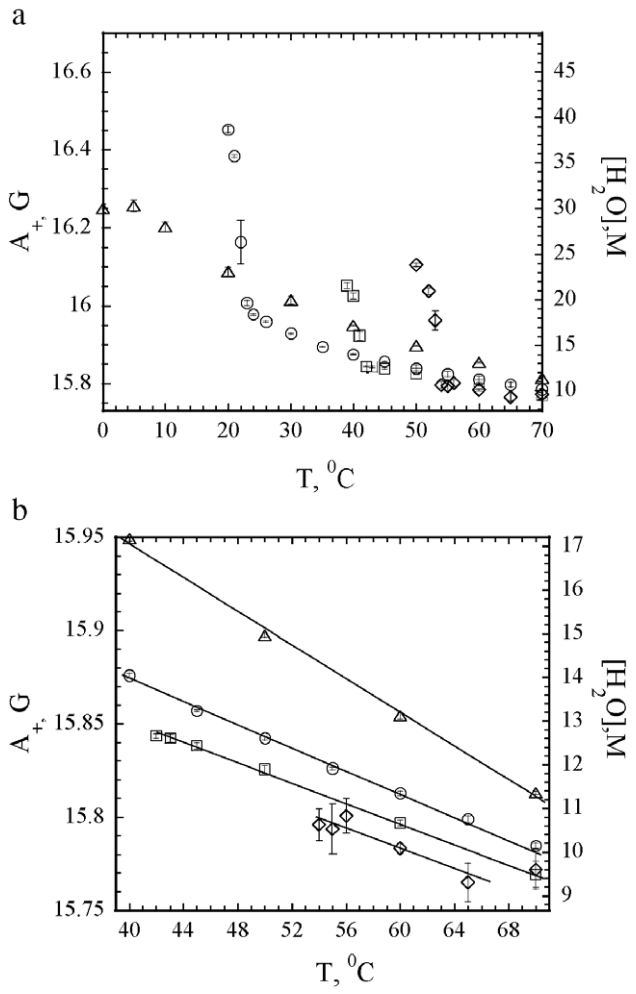

Fig. 4. (a) Nitrogen hyperfine spacing A_+ of 0.2 mM TEMPO-stearate in the presence of 100 mM of phospholipids in Hepes buffer equilibrated with N_2 at pH 7.4 (left-hand ordinate) and corresponding effective water concentration [H_2O] in the polar shell calculated from Eq. (11), (right-hand ordinate) as a function of temperature. Symbols used to identify the different phospholipids are: (○) DMPC, (□) DPPC, (◇) DSPC and (Δ) DOPC. Error bars are standard deviations of five measurements. (b) An expanded presentation of (a) at higher temperatures; lines are to guide the eyes.

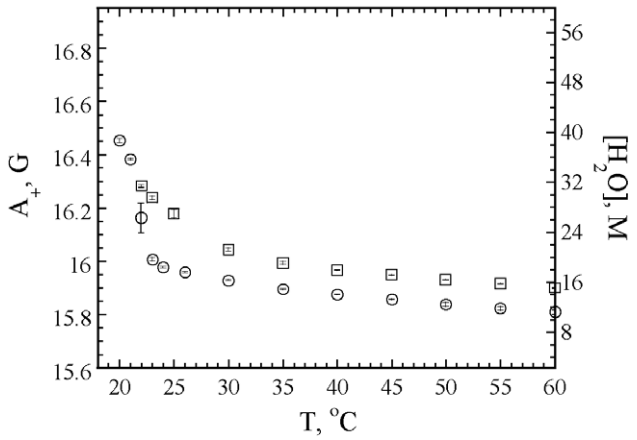

Fig. 5. Nitrogen hyperfine spacing A_+ of 0.2 mM TEMPO-stearate in the presence of 100 mM of phospholipids in Hepes buffer equilibrated with N_2 at pH 7.4 (left-hand ordinate) and corresponding effective water concentration [H_2O] in the polar shell calculated from Eq. (11), (right-hand ordinate) as a function of temperature. Symbols used to identify the different phospholipids are: (○) DMPC, (□) DMPG. Error bars are standard deviations of five measurements.

TEMPO-stearate. To gain further insight in how useful the effective concentration of water in the polar shell of the vesicle measured by this spin probe is, we compare the values of [H_2O] measured in DMPC and DMPG vesicles using TEMPO-stearate, Fig. 5. As expected, we can observe in Fig. 5 that DMPG vesicles are more hydrated than DMPC vesicles. Table 1 shows the effective water concentration in DMPG and DMPC vesicles measured by TEMPO-stearate, Fig. 5, and the spin probe di-*tert*-butyl nitroxide (DTBN), Figs. 3 and 5 from Ref. [24], at 40 °C. The value of [H_2O] measured by TEMPO-stearate is about 8 M greater than that measured by DTBN. This difference very likely comes from the different locations of the spin probes. DTBN is a small, mobile probe, and as such can sample the whole region of the polar shell, giving an average of the effective water concentration. TEMPO-stearate is anchored in the bilayer and senses only a limited region of the polar shell, and at 40 °C this region is closer to the vesicle's surface. At the higher temperatures TEMPO-stearate moves deeper and the average value of [H_2O] decreases. On the other side, one can see that the difference in effective water concentration between DMPG and DMPC vesicles measured by both spin probes is nearly constant.

The hydration properties of the water–phospholipid interface of phospholipids vesicles can also be studied by several other techniques including differential scanning calorimetry (DSC) [37], deuterium nuclear magnetic resonance (^{2}H NMR) [38,39] and X-ray methods [40,41]. Using the area per phospholipid for DMPC, DPPC and DSPC measured by ^{2}H NMR [39], and assuming that the thickness of the polar shell is 9 Å and the volume of the phosphatidylcholine headgroup is 331 Å^3 [40], we can immediately calculate the volume fraction of the polar shell [40] occupied by water. Again, due to the inability of our method to separate the effect of the polar shell hydration from the effect of location of TEMPO, our absolute values of the effective water concentration are different from those calculated from the area per lipid measured by the ^{2}H NMR and X-ray methods. However, the relative effective water concentrations correlate well with other methods. The difference between DMPC, DPPC and DSPC vesicles at 65 °C, which are 25.5, 25.0 and 24.5 M, respectively, is the same as the difference of 0.5 M measured by the EPR method, Fig. 4b. Also, our measurements indicate that this difference does not depend on temperature, Fig. 4b, which is the same as the conclusion derived from Fig. 8 in Ref. [39]. The difference in effective water concentration

Table 1
Effective water concentration in the polar shell of 100 mM DMPG and DMPC vesicle dispersions measured by TEMPO-stearate, Fig. 5, and DTBN, Figs. 3 and 5 from Ref. [23], at 40 °C

	[H_2O](DMPG)/M	[H_2O](DMPC)/M	Δ[H_2O] [a]/M
TEMPO-stearate	18.14	14.24	3.9
DTBN	10.24	6.59	3.65

[a] Δ[H_2O] = [H_2O](DMPG) − [H_2O](DMPC).

between DOPC and DMPC at 30 °C calculated from the area per lipid from Ref. [41] is 5.4 M while our value of 3.6 M is slightly lower. It is obvious that as long as we keep in mind the changing position of TEMPO-stearate and use vesicles of similar structure we can get useful information on the vesicle surface hydration.

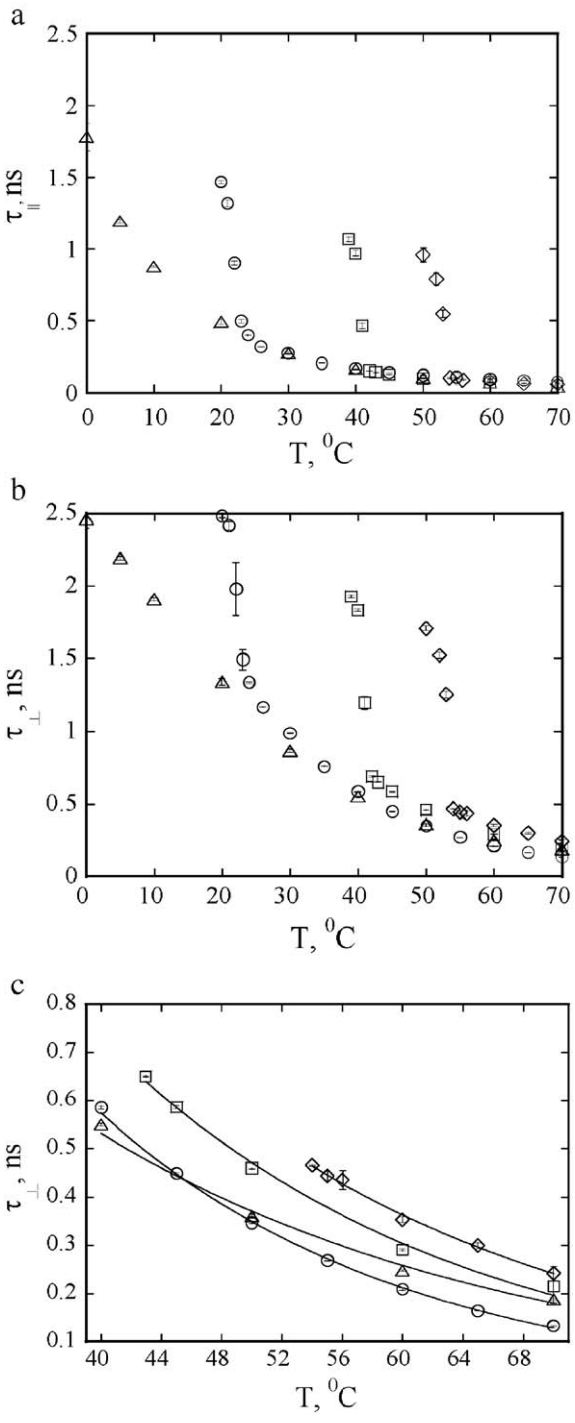

Fig. 6. (a) Rotational correlation time $\tau_{\parallel}$ and (b) rotational correlation time $\tau_{\perp}$ of 0.2 mM TEMPO-stearate in 100 mM phospholipid vesicles in Hepes buffer at pH 7.4 as a function of temperature. Symbols used identify the different phospholipids and are: (○) DMPC, (□) DPPC, (◇) DSPC and (Δ) DOPC. Error bars are standard deviations of three measurements. (c) An expanded presentation of (b) at higher temperatures; solid lines are exponential fits to the data.

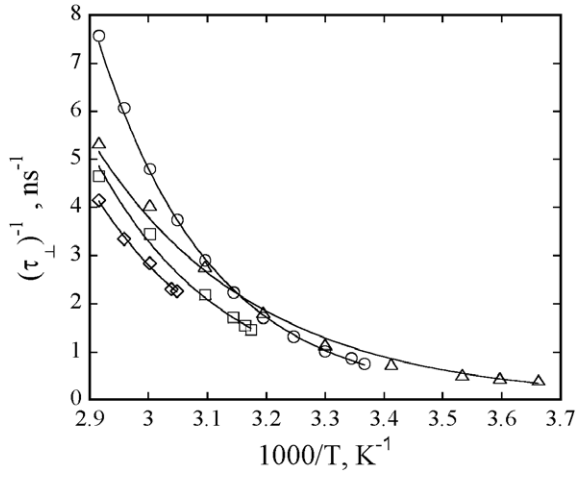

Fig. 7. The reciprocal of rotational correlation time $\tau_{\perp}$ of 0.2 mM TEMPO-stearate in 100 mM phospholipid vesicles in Hepes buffer at pH 7.4 as a function of temperature. Symbols used identify the different phospholipids and are: (○) DMPC, (□) DPPC, (◇) DSPC and (Δ) DOPC. Solid lines are exponential fits to the data, Eq. (12).

The rotational correlation times of TEMPO-stearate can give us additional information about the spin probe's environment. Fig. 6a shows the parallel rotational correlation time $\tau_{\parallel}$, characterizing the rotation about the hydrocarbon chain, for DMPC, DPPC, DSPC and DOPC vesicles as a function of temperature. Again, the phase transitions are well defined. As expected, the values of $\tau_{\parallel}$ abruptly decrease across the phase transition, but the values of $\tau_{\parallel}$ are the same for all phospholipids in the liquid crystal phase for a given temperature. The chain length affects only the temperature of phase transition, but once the system crosses this temperature the chain length does not affect the state of the cylindrical rotation of TEMPO-stearate. The perpendicular rotational correlation time $\tau_{\perp}$, characterizing the rotation of the nitroxide perpendicular the hydrocarbon chain, is presented in Fig. 6b. The value of $\tau_{\perp}$ is greater than the value of $\tau_{\parallel}$ for a given temperature, *x*-axis rotation, not a surprising result at all. Qualitatively, the behavior of $\tau_{\perp}$ is similar to that of $\tau_{\parallel}$, but, there is a small difference: the value of $\tau_{\perp}$ exhibits a slight but noticeable dependence on the chain length. From Fig. 6c it is obvious that the perpendicular correlation time becomes slightly longer with increasing chain length. A likely explanation for this increase is that as the chain length increases the hydrophobic interactions between the phospholipid chains increase. This in turn reduces the area per

Table 2
Activation energies of the perpendicular rotational correlation times for different phospholipid vesicles, Eq. (12)

Phospholipid	E_A, kJ/mol	Correlation coefficient
DMPC	42.7	0.999
DPPC	37.9	0.995
DSPC	38.0	0.998
DOPC	29.9	0.998
DMPG	47.4	0.999

phospholipid, which is in agreement with the decrease in area per lipid for the same phospholipids measured by the ^{2}H NMR [39] and X-ray methods [40]. The reduced area implies a decrease in water concentration, thus the decreased hydration more effectively restricts the perpendicular rotation of the nitroxide, prolonging the perpendicular rotational correlation time. The values of effective water concentration, Fig. 4b, support this interpretation. The effective water concentration in different phospholipid vesicles for a given temperature decreases with increasing chain length, indicating a decrease in area per phospholipid with chain length. The decrease of effective water concentration is about 0.5 M for an increase of two carbons in the chain.

The solid lines in Fig. 6c, which are exponential fits to the experimental data, clearly show that the perpendicular rotational correlation time for each phospholipid above the phase transition exhibits exponential temperature dependence. To find the activation energy E_A for the perpendicular rotation of TEMPO it is necessary to use the well-known Arrhenius equation:

$$\frac{1}{\tau_\perp} = Ae^{-\frac{E_A}{RT}} \tag{12}$$

Fig. 7 shows the reciprocal of $1/\tau_\perp$ as a function of $1000/T$, where solid lines are fits to Eq. (12). The activation energies extracted from the fits are given in Table 2. The activation energy of 29.9 kJ/mol for TEMPO in DOPC vesicles is very close to the activation energy of the fatty acid spin label I(13, 2) (5 doxylstearic acid) in a decanol-sodium decanoate bilayer, 28.6 kJ/mol [42], and the activation energy of the spin probe 16-doxylstearic acid methyl ester in tetraalkylammonium dodecyl sulfate micelles, 29.3 kJ/mol [43]. This similarity implies that the polar shell of DOPC vesicles is a normal liquid mixture, not very different from above mentioned liquids. The activation energy for saturated phospholipid DSPC vesicles is 8 kJ/mol greater, indicating that the rotation of NO· in the polar shell of those vesicles is more restricted.

The parallel and perpendicular rotational correlation times above 30 °C as a function of temperature in both DMPG and DMPC vesicles are shown in Fig. 8. The value of $\tau_\perp$ in DMPG vesicles is shorter, indicating that the area per lipid is greater in DMPG vesicle than in DMPC vesicles due to higher hydration, as expected. On the other side, the value of $\tau_\parallel$ is larger in DMPG vesicles than in DMPC vesicles. Also, the activation energy for DMPG vesicles is larger than for DMPC vesicles, Table 2. A possible explanation for these differences might be that the number of hydrogen bonds in the polar shell of DMPG vesicles is greater than in the polar shell of DMPC vesicles [44]. Thus, the increased hydrogen bond network retards the cylindrical rotation of the nitroxide.

DOPC has unsaturated chains, so the DOPC vesicles are expected to have higher fluidity of the bilayer and a more hydrated polar shell than the phospholipid with the same chain length, DSPC. The observed data fully support this line of argument. Fig. 4a and b shows that the effective water concentration in DOPC vesicles in the liquid crystal phase is higher than in DSPC vesicles at a given temperature. Also, the perpendicular rotational correlation time is shorter in DOPC vesicles, Fig. 6c, indicating again an increased area per lipid.

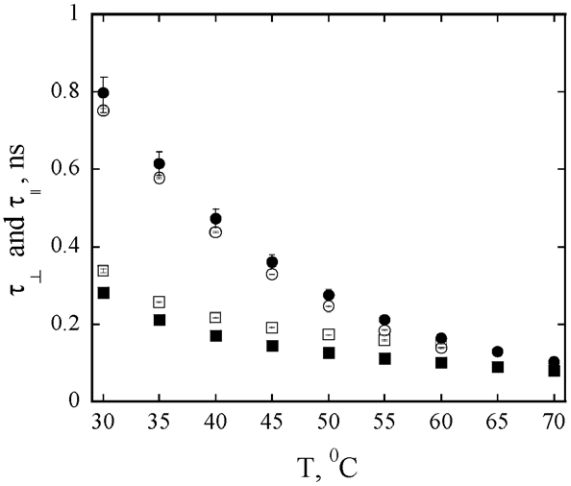

Fig. 8. Rotational correlation times $\tau_\parallel$ and $\tau_\perp$ of 0.2 mM TEMPO-stearate in 100 mM phospholipid vesicles in Hepes buffer at pH 7.4 as a function of temperature above phase transition. Symbols used to identify different times and phospholipids are: $\tau_\perp$ — (○) DMPG and (●) DMPC; and $\tau_\parallel$ — (□) DMPG and (■) DMPC.

4. Conclusions

We have clearly shown that nonlinear least-squares spectral fitting applied to the EPR spectrum of the spin probe TEMPO-stearate in phospholipid vesicles above the phase transition yields EPR parameters of high precision, which can then be used to construct a detailed picture of the motion of the nitroxide moiety. At the same time, information on the hydration of the spin probe environment can be obtained. The effective water concentration values and rotational correlation times indicate that the spin probe position probably moves a few angstroms across the phase transition, which can be used to measure the temperature of the phase transition of lipid vesicles. The experimental results show that the polar shell of the negatively charged DMPG vesicles is more hydrated than that of the zwitterionic DMPC vesicles. Also, the hydration of the vesicle surface decreases with hydrocarbon chain length, as well as with the unsaturation of the hydrocarbon chains. The effect of chain length on the vesicle surface hydration is less pronounced than the effect of the polarity of the phospholipid head and the unsaturation of the hydrocarbon chains.

Acknowledgments

The authors gratefully acknowledge support from NIH Grant 3 S06 GM48680-10S1 (MA and MP). We also acknowledge valuable discussions with Dr. Barney L. Bales.

References

[1] L.R. Dalton, EPR and Advanced EPR Study of Biological Systems, CRC Press, Boca Raton, 1984.

[2] J.L. Berliner, J. Reuben, Spin labeling: theory and applications, Biological Magnetic Resonance, Plenum Press, New York, 1989.
[3] P.F. Devaux, P. Felmann, P. Hervé, Investigation on lipid asymmetry using lipid probes comparison between spin-labeled lipids and fluorescent lipids, Chem. Phys. Lipids 116 (2002) 115–134.
[4] A. Baszkin, W. Norde, Physical Chemistry of Biological Interfaces, Marcel Dekker, New York, 2000.
[5] G. Cevc, Phospholipids Handbook, Marcel Dekker, New York, 1993.
[6] K.I. Florine, G.W. Feigenson, Influence of the calcium-induced gel phase on the behavior of small molecules in phosphatidylserine and phosphatidylserine–phosphatidylcholine multilamellar vesicles, Biochemistry 26 (1987) 1757–1768.
[7] R. Bartucci, G. Montesano, L. Sportelli, Effects of poly(ethylene glycol) on neutral lipid bilayers, Colloids Surf., A 115 (1996) 63–71.
[8] J.-J. Yin, M.J. Smith, R.M. Eppley, A.L. Troy, S.W. Page, J.A. Sphon, Effects of fumonisin B_1 and (hydrolyzed) fumonisin backbone AP_1 on membranes: a Spin-Label Study, Arch. Biochem. Biophys. 335 (1996) 13–22.
[9] S. Belsito, R. Bartucci, L. Sportelli, Sterically stabilized liposomes of DPPC DPPE-PEG:2000. A Spin Label ESR and Spectrophotometric Study, Biophys. Chem. 75 (1998) 33–43.
[10] A.B. Hendrich, O. Wesolowska, M. Komorowska, N. Motohashi, K. Michalak, The alterations of lipid bilayer fluidity induced by newly synthesized phenothiazine derivative, Biophys. Chem. 98 (2002) 275–285.
[11] A. Caragheorgheopol, H. Caldararu, EPR spin-labelling and spin-probe studies of self-assembled systems, in: M.J. Davies, K.A. Mclauchlan (Eds.), Electron Paramagnetic Resonance, Royal Society of Chemistry, Cambridge, 2000.
[12] H.J. Halpern, M. Peric, C. Yu, B.L. Bales, Rapid quantitation of parameters from inhomogeneously broadened EPR spectra, J. Magn. Reson. A103 (1993) 13–22.
[13] A.I. Smirnov, R.I. Belford, Rapid quantitation from inhomogeneously broadened EPR spectra by a fast convolution algorithm, J. Magn. Reson., A 113 (1995) 65–73.
[14] B.L. Bales, M. Peric, EPR line shifts and line shape changes due to spin exchange of nitroxide free radicals in liquids, J. Phys. Chem., B 101 (1997) 8707–8716.
[15] B.H. Robinson, C. Mailer, A.W. Reese, Linewidth analysis of spin labels in liquids; I Theory and data analysis, J. Magn. Reson. 138 (1999) 199–209.
[16] B.L. Bales, Inhomogeneously broadened spin-label spectra, in: J.L. Berliner, J. Reuben (Eds.), Spin Labeling Theory and Applications, Plenum, New York, 1989, pp. 77–130.
[17] M. Peric, B.L. Bales, Lineshapes of spin exchange broadened EPR spectra, J. Magn. Reson. 169 (2004) 27–29.
[18] B.L. Bales, L. Messina, A. Vidal, M. Peric, O.R. Nascimento, Precision relative aggregation number determinations of SDS micelles using a spin probe. A model of micelle surface hydration, J. Phys. Chem., B 102 (1998) 10347–10358.
[19] B.L. Bales, R.L. Ranganathan, P.C. Griffiths, Characterization of mixed micelles of SDS and a sugar-based nonionic surfactant as a variable reaction medium, J. Phys. Chem., B 105 (2001) 7465–7473.
[20] R. Ranganathan, M. Peric, R. Medina, U. Garcia, B.L. Bales, M. Almgren, Size, hydration, and shape of SDS/heptane micelles investigated by time-resolved fluorescence quenching and electron spin resonance, Langmuir 17 (2001) 6765–6770.
[21] D.J. Schneider, J.H. Freed, Calculating slow motional magnetic resonance spectra, in: J.L. Berliner, J. Reuben (Eds.), Biological Magnetic Resonance, Plenum, New York, 1989, pp. 1–76.
[22] D.E. Budil, S. Lee, S. Saxena, Nonlinear-least-squares analysis of slow-motion EPR spectra in one and two dimensions using modified Levenberg–Marquardt algorithm, J. Magn. Reson., A 120 (1996) 155–189.
[23] A.I. Smirnov, T.I. Smirnova, P.D. Morse, Very high frequency electron paramagnetic resonance of 2,2,4,4-tetramethyl-1-piperidnyloxy in 1,2-dipalmitoyl-sn-glycero-3-phosphatidylcholine liposomes: partitioning and molecular dynamics, Biophys. J. 68 (1995) 2350–2360.
[24] M. Peric, M. Alves, B.L. Bales, Precision parameters from spin-probe studies of membranes using a partitioning technique. Application to two model membrane vesicles, Biochim. Biophys. Acta 1669 (2005) 116–124.
[25] W.Z. Plachy, D.A. Windrem, A gas-permeable ESR sample tube, J. Mag. Reson. 27 (1977) 237–239.
[26] B.L. Bales, M. Peric, EPR line shifts, and line shape changes due to spin exchange of nitroxide free radicals in liquids 2. Extension to high spin exchange frequencies and inhomogeneously broadened spectra, J. Phys. Chem., A 106 (2002) 4846–4854.
[27] S. Schreier, C.F. Polnaszek, I.C.P. Smith, Spin labels in membranes problems in practice, Biochim. Biophys. Acta 515 (1978) 375–436.
[28] D. Marsh, Experimental methods in spin-label spectral analysis, in: L.J. Berliner, J. Reuben (Eds.), Spin Labeling Theory and Applications, Plenum, New York, 1989, pp. 255–303.
[29] M. Tabak, A. Alonso, O.R. Nascimento, Single crystal ESR studies of a nitroxide spin label: I. Determination of G and A tensors, J. Chem. Phys. 79 (1983) 1176–1184.
[30] D. Marsh, Handbook of Lipid Bilayers, CRC Press, Boca Raton, 1990.
[31] C.C. Wang, R. Pecora, Time-correlation function for restricted rotational diffusion, J. Chem. Phys. 72 (1980) 5333–5340.
[32] A. Kusumi, M. Pasenkiewicz-Gierula, Rotational diffusion of a steroid molecule in phosphatidylcholine membranes: effects of alkyl chain length, unsaturation, and cholesterol as studied by a spin-label method, Biochemistry 27 (1988) 4407–4415.
[33] M. Pasenkiewicz-Gierula, W.K. Subczynski, A. Kusumi, Rotational diffusion of a steroid molecule in phosphatidylcholine-cholesterol membranes: fluid-phase microimmiscibility in unsaturated phosphatidylcholine-cholesterol membranes, Biochemistry 29 (1990) 4059–4069.
[34] O.H. Griffith, P.J. Dehlinger, S.P. Van, Shape of the hydrophobic barrier of phospholipid bilayers (evidence for water penetration in biological membranes), J. Membr. Biol. 15 (1974) 159–192.
[35] P. Mukerjee, C. Ramachandran, R.A. Pyter, Solvent effects on the visible spectra of nitroxides and relation to nitrogen hyperfine splitting constants. Nonempirical polarity for aprotic and hydroxilic solvents, J. Phys. Chem. 86 (1982) 3189–3197.
[36] J. Kristla, B. Volka, M. Gasperlina, M. Sentjurc, J.P., Effect of colloidal carriers on ascorbyl palmitate stability, Eur. J. Pharm. Sci. 19 (2003) 181–189.
[37] D. Bach, I.R. Miller, Hydration of phospholipid bilayers in the presence and absence of cholesterol, Biochim. Biophys. Acta 1368 (1998) 216–224.
[38] C. Faure, L. Bonakdar, E.J. Dufourc, Determination of DMPC hydration in the L_α and $L_{\beta'}$ Phases by ^2H solid state NMR of D_2O, FEBS Lett. 405 (1997) 263–266.
[39] H.I. Petrache, S.W. Dodd, M.F. Brown, Area per lipid and acyl length distributions in fluid phosphatidylcholines determined by ^2H NMR spectroscopy, Biophys. J. 79 (2000) 3172–3192.
[40] N. Kucerka, Y. Liu, N. Chu, H.I. Petrache, S. Tristram-Nagle, J.F. Nagle, Structure of fully hydrated fluid phase DMPC and DLPC lipid bilayers using X-ray scattering from oriented multilamellar arrays and from unilamellar vesicles, Biophys. J. 88 (2005) 2626–2637.
[41] N. Kucerka, S. Tristram-Nagle, J.F. Nagle, Structure of Fully Hydrated Fluid Phase Lipid Bilayers with Monounsaturated Chains, J. Membr. Biol. (accepted).
[42] H. Schindler, J. Seelig, EPR spectra of spin labels in lipid bilayers, J. Chem. Phys. 59 (1973) 1841–1850.
[43] B.L. Bales, M. Benrraou, T. Tiguida, R. Zana, Effect of the nature of the counterion on the properties of anionic surfactants: 4. Characterizing micelles of tetraalkylammonium dodecyl sulfate as reaction media, J. Phys. Chem., B 109 (2005) 7987–7997.
[44] M. Pasenkiewicz-Gierula, Y. Takaoka, H. Miyagawa, K. Kitamura, A. Kusumi, Hydrogen bonding of water to phosphatidylcholine in the membrane as studied by a molecular dynamics simulation: location, geometry, and lipid–lipid bridging via hydrogen-bonded water, J. Phys. Chem., A 101 (1997) 3677–3691.